Notch signaling in vascular smooth muscle cells is required to pattern the cerebral vasculature

Aaron Proweller*†, Alex C. Wright‡, Debra Horng‡, Lan Cheng†, Min Min Lu†, John J. Lepore*†, Warren S. Pear§¶‖, and Michael S. Parmacek*†**

Departments of *Medicine, ‡Radiology, and §Pathology and Laboratory Medicine, ¶Abramson Cancer Center, ‖Institute for Medicine and Engineering, and †Cardiovascular Institute, University of Pennsylvania, Philadelphia, PA 19104

Communicated by Mark T. Keating, Novartis Institutes for Biomedical Research, Inc., Cambridge, MA, August 24, 2007 (received for review June 26, 2007)

Stroke is the third leading cause of death and a significant contributor of morbidity in the United States. In humans, suboptimal cerebral collateral circulation within the circle of Willis (CW) predisposes to ischemia and stroke risk in the setting of occlusive carotid artery disease. Unique genes or developmental pathways responsible for proper CW formation are unknown. Herein we characterize a mouse model lacking Notch signaling in vascular smooth muscle cells (vSMCs), in which the animals are intolerant to reduced cerebral blood flow. Remarkably, unilateral carotid artery ligation results in profound neurological sequelae and death. After carotid ligation, perfusion of the ipsilateral cerebral hemisphere was markedly diminished, suggesting an anastomotic deficiency within the CW. High-resolution microcomputed tomographic (μ-CT) imaging revealed profound defects in cerebrovascular patterning, including interruption of the CW and anatomic deformity of the cerebral arteries. These data identify a vSMC-autonomous function for Notch signaling in patterning and collateral formation within the cerebral arterial circulation. The data further implicate genetic or functional deficiencies in Notch signaling in the pathogenesis of anatomic derangements underlying cerebrovascular accidents.

angiogenesis | cerebrovascular accident | vascular patterning | mastermind

Signaling through multiple Notch receptors is required for normal mammalian vascular development and postnatal vessel maturation. Critical functions for Notch ligands and their receptors have been identified in endothelial cells (1–4). Although multiple Notch receptors are expressed in vascular smooth muscle cells (vSMCs) (5), a cell-autonomous role for Notch signaling in these cells remains undefined. In canonical Notch signaling, binding of transmembrane Notch receptors (N1–N4) by Jagged or Delta ligands results in γ-secretase-mediated cleavage and release of the Notch intracellular domain, its nuclear translocation and association with the transcriptional-activator Mastermind, and DNA-binding protein, CSL/RBP-J (6). This heterotrimeric complex induces the expression of Notch target genes, including members of the basic helix–loop–helix family of Hairy-related transcription factors (HRTs) (7).

The cerebrovascular circulation has evolved unique mechanisms to preserve homeostasis and tissue perfusion despite variations in blood pressure and volume. Cerebral ischemia is poorly tolerated, and prolonged disruption of blood flow causes irreversible brain injury and concomitant neurological deficits. In higher vertebrates, the cerebral circulation is derived from the carotid and vertebral-basilar arteries that communicate at the circle of Willis (CW). The CW comprises the primary collateral network that preserves cerebral perfusion when blood flow from the carotid or vertebral arteries is interrupted. Anatomic deformities within the CW significantly increase the risk of stroke in patients undergoing common surgical procedures involving the carotid arteries and aorta (8–16). Anatomic variations in the CW have been observed in ≈50% of patients, predisposing them to stroke (17, 18). However, little is currently understood about the molecular and genetic programs that regulate patterning of the cerebral arteries and the CW.

In the studies described in this report, we generated conditional transgenic mice in which canonical Notch signaling in vSMCs is abolished. Surprisingly, these mutant transgenic mice are viable, are fertile, and do not exhibit an obvious cardiovascular phenotype. However, when the Notch-mutant mice are subjected to unilateral carotid injury, they exhibit profound neurological deficits. Microcomputed tomographic (μ-CT) angiography revealed marked defects in cerebrovascular patterning, including interruption of the CW. These data provide insights into the molecular and genetic programs that regulate cerebrovascular patterning, and they provide a conceptual framework for examining genetic predisposition to stroke and cerebrovascular pathologies in humans.

Results

Conditional Inactivation of Notch Signaling in vSMCs. To determine the function of CSL-dependent Notch signaling in vSMCs and to circumvent potentially redundant functions of Notch receptors, SM22-Cre$^+$/DNMAML1$^+$ mice were characterized in which the pan-Notch inhibitor, Dominant-Negative MasterMind-Like 1 (DNMAML1), was expressed in an SMC lineage-restricted fashion (Fig. 1*A*). DNMAML1 binds the Notch intracellular domain:CSL dimer, but fails to recruit critical transcriptional coactivators, thus preventing Notch-induced transcriptional activation (19–21). Experiments in lymphocytes showed that DNMAML inhibits signaling by all four Notch receptors and phenocopies loss of both individual Notch receptors and CSL (22). SM22-Cre$^+$/DNMAML1$^+$ mice are born in predicted Mendelian ratios, display normal behavior, but have reduced growth rates, and exhibit progressive alopecia compared with littermate controls (Fig. 1*A*) (20). EGFP staining indicative of DNMAML1 expression was detected in vSMCs in aorta and cerebral vasculature, as well as in visceral smooth muscle of the bladder (Fig. 1*B*). Furthermore, Jagged-1-induced expression of *HRT1*, *HRT2*, and *HRT3* was observed in cultured primary aortic SMCs harvested from SM22-Cre$^-$/DNMAML1$^+$ control mice, but not in aortic SMCs harvested from SM22-Cre$^+$/DNMAML1$^+$ mice. This result demonstrates that Notch signal-

Author contributions: A.P. and M.S.P. designed research; A.P., D.H., L.C., M.M.L., and M.S.P. performed research; A.P., J.J.L., and W.S.P. contributed new reagents/analytic tools; A.P., A.C.W., W.S.P., and M.S.P. analyzed data; and A.P., A.C.W., W.S.P., and M.S.P. wrote the paper.

The authors declare no conflict of interest.

Abbreviations: ACA, anterior cerebral artery; AComA, anterior communicating artery; A-V, arterial-venous; CW, circle of Willis; DNMAML1, dominant-negative mastermind-like 1; HRT, Hairy-related transcription factor; LCCA, left common carotid artery; MCA, middle cerebral artery; RCCA, right common carotid artery; μ-CT, microcomputed tomography; vSMC, vascular smooth muscle cell.

**To whom all correspondence should be addressed. E-mail: michael.parmacek@uphs.upenn.edu.

This article contains supporting information online at www.pnas.org/cgi/content/full/0707950104/DC1.

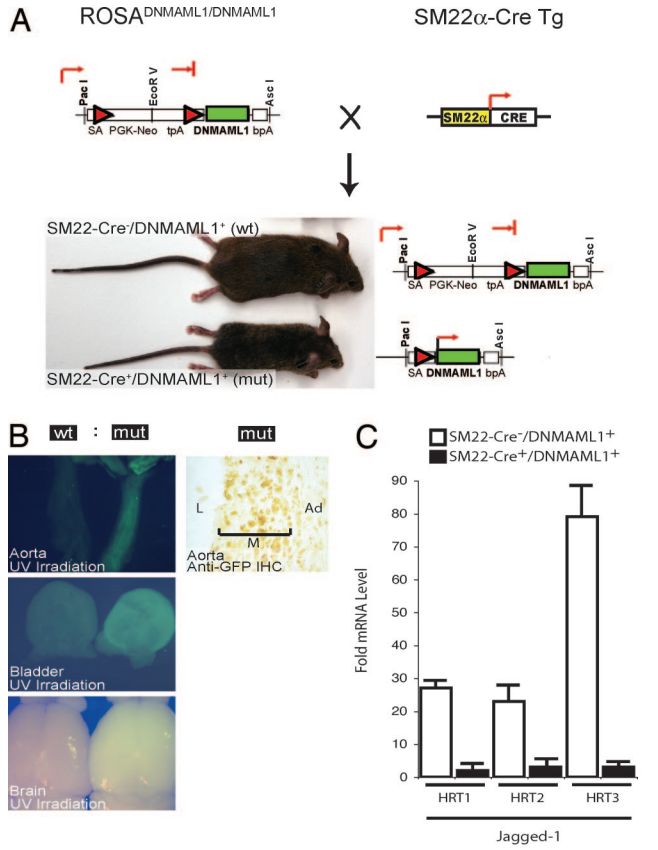

Fig. 1. SM22-Cre$^+$/DNMAML1$^+$ mice repress Notch signaling in vSMCs. (*A*) Generation of SM22-Cre$^+$/DNMAML1$^+$ progeny from intercrossing ROSA$^{D\text{-}NMAML1/DNMAML1}$ and SM22α-Cre transgenic mice. DNMAML1 is a fusion of DNMAML1 peptide with EGFP. Cre recombinase removes a PGK-Neo-stop codon cassette allowing read-through transcription and expression of DNMAML1 by the ROSA promoter. SM22-Cre$^+$/DNMAML1$^+$ mice exhibit reduced body mass relative to SM22-Cre$^-$/DNMAML1$^+$ littermate controls. (*B*) DNMAML1 expression in vascular and visceral smooth muscle-containing organs from SM22-Cre$^+$/DNMAML1$^+$ mice. UV-induced green fluorescence in brain results from the expression of DNMAML1 in the dense cerebral-cortical vasculature. Anti-GFP immunohistochemistry reveals nuclear localization of DNMAML1 in aortic vSMCs. L, lumen; M, media; Ad, adventia. (*C*) DNMAML1 inhibits Jagged-1-induced Notch target gene expression. Primary aortic SMCs derived from SM22-Cre$^+$/DNMAML1$^+$ and SM22-Cre$^-$/DNMAML1$^+$ littermate control mice were exposed to Jagged-l ligand for 48 h. cDNA prepared from harvested RNA was subjected to real-time PCR to monitor transcript levels of CSL-dependent Notch target genes *HRT1*, *HRT2*, and *HRT3* relative to the expression of GAPDH mRNA. Data are displayed as -fold mRNA levels induced by Jagged-1 relative to values obtained from vSMC exposed only to Fc fused to TRAIL-R4 extracellular domain (negative control) (data not shown) and are representative of multiple experiments.

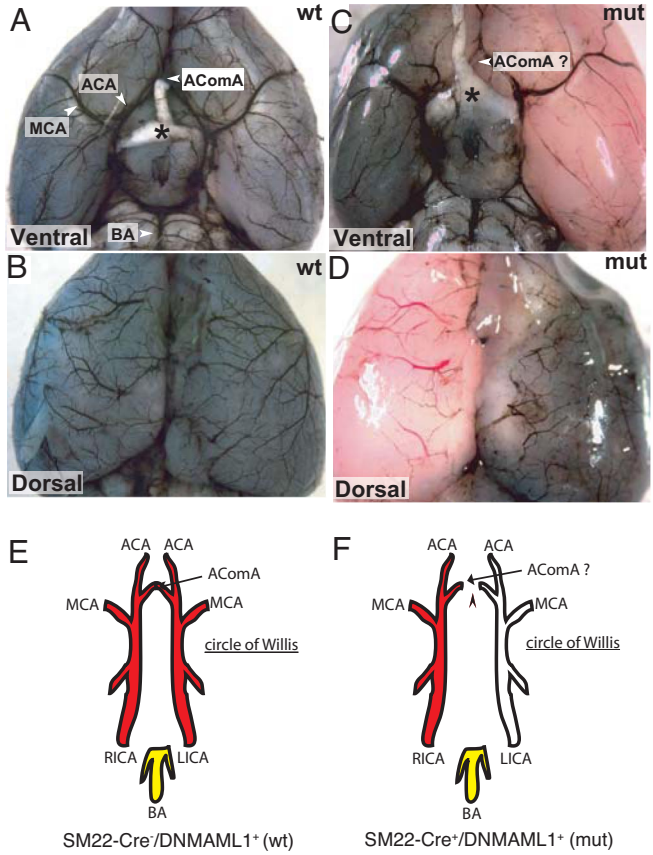

Fig. 2. Cerebrovascular perfusion defect in SM22-Cre$^+$/DNMAML1$^+$ mice after LCCA ligation. (*A* and *B*) Ventral and dorsal views, respectively, of a representative control SM22-Cre$^-$/DNMAML1$^+$ mouse brain perfused with carbon black ink by left-ventricular cardiac injection in the presence of LCCA ligation. Ink opacification of cerebral-cortical vasculature is clearly observed throughout both cerebral hemispheres. (*C* and *D*) Ventral and dorsal views, respectively, of a representative mutant SM22-Cre$^+$/DNMAML1$^+$ mouse brain perfused with carbon black ink as in *A* and *B* in the presence of LCCA ligation. There is markedly diminished carbon black perfusion of the left (ipsilateral) cerebral hemisphere. (*E* and *F*) CW anatomy in control SM22-Cre$^-$/DNMAML1$^+$ mice (*E*), and a model predicting defective collateral formation (absent AComA segments) in the anterior portion of the CW in mutant SM22-Cre$^+$/DNMAML1$^+$ mice (*F*). ACA, anterior cerebral artery; AComA, anterior communicating artery; MCA, middle cerebral artery; BA, basilar artery; *, optic chiasm; RICA; right internal carotid artery; LICA, left internal carotid artery.

ing is functionally repressed by DNMAML1 in vSMCs of SM22-Cre$^+$/DNMAML1$^+$ mice (Fig. 1*C*).

Neurological Sequelae and Diminished Cerebral Perfusion After Unilateral Carotid Ligation. To examine the functions of Notch signaling after acute vascular injury, SM22-Cre$^+$/DNMAML1$^+$ mice and control littermates were subjected to left common carotid artery (LCCA) ligation. However, during recovery from surgical anesthesia, the SM22-Cre$^+$/DNMAML1$^+$ mice unexpectedly displayed profound motor deficits, including difficulty maintaining balance and a clockwise rolling motion [supporting information (SI) Movie 1]. The majority (92%, $n = 12$) of SM22-Cre$^+$/DNMAML1$^+$ mice died within 24 h postprocedure, and in some animals ($n = 4$) death occurred within a few hours.

All ($n = 12$) littermate control mice displayed normal postoperative recovery, including full motor function. The motor deficits displayed by SM22-Cre$^+$/DNMAML1$^+$ mice suggested inadequate cerebral perfusion of the ipsilateral (left) cerebral hemisphere. Intracardiac injection of carbon black ink after LCCA ligation in control mice revealed black ink in the arteries supplying both the right and left sides of the brain, including the pial and cortical vessels (Fig. 2 *A* and *B*). However, in SM22-Cre$^+$/DNMAML1$^+$ mice, markedly diminished perfusion of the left (ipsilateral) cerebral hemisphere was observed, whereas the arterial supply of the contralateral hemisphere was indistinguishable from control mice (Fig. 2 *C* and *D*). This observation strongly suggests that arteries or collateral vessels connecting the right and left cerebral hemispheres were either absent or nonfunctional in SM22-Cre$^+$/DNMAML1$^+$ mice, implicating a disruption at the level of the CW (Fig. 2 *E* and *F*). Consistent with this model, unilateral right common carotid artery (RCCA) ligation in SM22-Cre$^+$/DNMAML1$^+$ mice resulted in disrupted perfusion of the right (ipsilateral) cerebral hemisphere, but not the left cerebral hemisphere ($n = 4$) (data not shown).

Fig. 3. μ-CT imaging reveals abnormal patterning of the CW and cerebral arteries in SM22-Cre$^+$/DNMAML1$^+$ mice. (*A* and *B*) Vascular anatomy of the CW in control SM22-Cre$^-$/DNMAML1$^+$ mouse brain in the presence (*A*, +L) or absence (*B*, −L) of RCCA ligation. Right and left anterior communicating arterial segments (AComA) are easily identified (encircled region in red and magnified in *Inset*). Note the symmetry and relative small size of arteries comprising the CW and at cerebral artery bifurcation sites (MCA/ACA). (*C* and *D*) Vascular anatomy of the CW and cerebral arteries of mutant SM22-Cre$^+$/DNMAML1$^+$ mice in the presence (*C*, +L) or absence (*D*, −L) of RCCA ligation. With ligation (*C*), there is minimal perfusion of the ipsilateral (right) cerebral vasculature (i.e., right-sided filling defect) and a notable absence of AComA segment opacification (red circle region and magnified in *Inset*). Without carotid ligation (*D*), there is bilateral filling of the CW, but once again communication between the right and left AComA is absent (red circle region and magnified in *Inset*). Note the asymmetric angioarchitecture of the CW and at cerebral artery bifurcation sites (MCA/ACA), as well as the dilation and constriction of arterial segments of the CW. (*E–G*) Absent anastomosis within the anterior CW from noncarotid artery-ligated (−L) mutant SM22-Cre$^+$/DNMAML1$^+$ mice in contrast to a littermate control mouse. ACA, anterior cerebral artery; AComA, anterior communicating artery; MCA, middle cerebral artery; BA, basilar artery (SM22-Cre$^+$/DNMAML1$^+$, $n = 7$; SM22-Cre$^-$/DNMAML1$^+$, $n = 9$).

Aberrant Cerebrovascular Patterning and Disruption of the CW in Notch-Mutant Mice. To define the cerebral arterial anatomy without disrupting the carotid and vertebral circulations, SM22-Cre$^+$/DNMAML1$^+$ and littermate control mice were analyzed by high-resolution μ-CT brain imaging after injection of intravascular contrast. Visualization of $\geq$16-μm-diameter vessels was achieved by 3D volume renderings of the cerebral arterial vasculature (SI Movie 2). In littermate control mice after RCCA ligation, contrast media uniformly filled the basilar and internal carotid artery circulations, including the CW and major cerebral arteries [middle cerebral artery (MCA) and anterior cerebral artery (ACA)] (Fig. 3*A*). Obvious anastomosis was observed between the right and left ACAs of the CW (Fig. 3*A Inset*). The arterial network in control mice was symmetric, including at sites of arterial bifurcation (e.g., MCA and ACA). Arterial caliber was relatively small and uniform within segments of the CW and within the proximal course of the major cerebral arteries. Vascular connections between the vertebral-basilar system and CW proper were not identified in control mice, consistent with previous reports demonstrating an absent or diminutive posterior communicating artery in many mouse strains (23–26). Identical patterning of the vasculature was observed in μ-CT

brain images of littermate control mice without carotid ligation, confirming intact anterior segment anastomoses within the CW (Fig. 3*B*).

In SM22-Cre$^+$/DNMAML1$^+$ mutant mice subjected to RCCA ligation, μ-CT imaging revealed filling of the left (contralateral) side of the CW and left-sided cerebral arteries, as well as the basilar artery (Fig. 3*C*). By contrast, only mild opacification was observed in right-sided cerebral arteries, demonstrating a lack of functional communication between the right and left cerebral circulations in SM22-Cre$^+$/DNMAML1$^+$ mutant mice. Moreover, in contrast to their control littermates, anastomoses between right and left ACAs in the anterior CW could not be demonstrated (Fig. 3 *D–G*). In addition, there was a generalized loss of arterial symmetry within the CW and in the cerebral arteries of the mutant mice. Branching at the bifurcations of the MCA and ACA from the CW was markedly asymmetric (compare Fig. 3 *D* to *B*). Finally, marked heterogeneity of the caliber of the cerebral arteries was noted in SM22-Cre$^+$/DNMAML1$^+$ mutant mice with variable dilation and constriction of arterial segments (Fig. 3*D*). In summary, patterning of the anterior CW (and other arteries) is markedly altered in SM22-Cre$^+$/DNMAML1$^+$ mutant mice, effectively disrupting arterial communication between the right and left cerebral hemispheres.

Abnormalities in Arterial Anatomy and Vessel Maturation. Notch signaling has been implicated in arterial-venous (A-V) patterning in zebrafish and mouse mutants (27, 28). The dilated and nonuniform caliber arteries of SM22-Cre$^+$/DNMAML1$^+$ mutant mice resembled venous structures. Histological analysis of control arteries revealed uniform, small-caliber lumens surrounded by multiple smooth muscle layers comprising the tunica media (Fig. 4 *A–C*, *G*, and *H*). By contrast, analogous arterial segments harvested from SM22-Cre$^+$/DNMAML1$^+$ mutant mice revealed arterial dilation with marked thinning of the tunica media more closely resembling venous anatomy (Fig. 4 *D–F*, *I*, and *J*). To determine whether A-V identity was altered in Notch-mutant mice, the expression of ephrin B2 and eph B4, which is present in both endothelial cells and vSMCs of arteries and veins, respectively (29), was examined. As anticipated, the expression of ephrin B2 and eph B4 distinguished arteries and veins in SM22-Cre$^-$/DNMAML1$^+$ control mice (Fig. 4 *K* and *N*). By contrast, ephrin B2 was not observed within vSMCs populating the tunica media of cerebral arteries in SM22-Cre$^+$/DNMAML1$^+$ mutant mice (Fig. 4*L*). Interestingly, expression of the venous marker, eph B4, also was not observed in these vessels (Fig. 4*O*). Absence of ephrin B2 staining was observed in cerebral arteries of SM22-Cre$^+$/DNMAML1$^+$ mutant mice at least as early as embryonic day 16.5, strongly suggesting that Notch signaling in vSMCs provides instructional cues required for arterial SMC maturation during embryonic development, which extends into adulthood (data not shown). Taken together, these results strongly suggest that inhibition of canonical Notch signaling in vSMCs results in defective arterial maturation and modulation of vessel identity markers in association with profound arterial patterning defects of the cerebral vasculature.

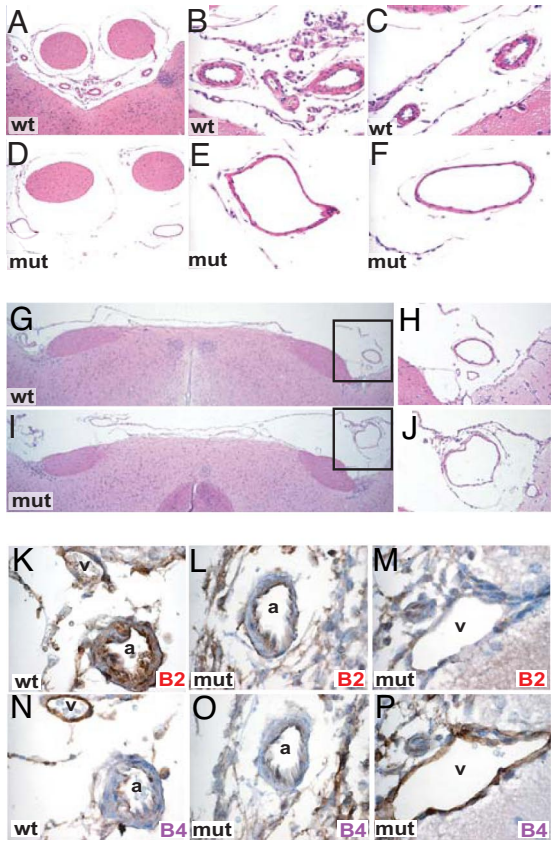

Fig. 4. Defective cerebral arterial maturation in SM22-Cre$^+$/DNMAML1$^+$ mice. (*A–F*) Cross-sectional analysis of corresponding anterior forebrain vasculature in control (*A*, magnified in *B* and *C*) and mutant SM22-Cre$^+$/DNMAML1$^+$ (*D*, magnified in *E* and *F*) mice. Mutant arteries exhibit larger luminal diameters and reduced thickness of the tunica media compared with control littermate vessels. (*G–J*) Cross-sectional vessel analysis at mid-CW in wild-type (*G*, box magnified in *H*) and mutant SM22-Cre$^+$/DNMAML1$^+$ (*I*, box magnified in *J*) mice. Mutants display asymmetric flanking segments of the CW, as well as larger overall diameter and reduced medial layer thickness compared with wild-type controls. (*K–P*) Reduced expression of smooth muscle arterial identity marker in SM22-Cre$^+$/DNMAML1$^+$ cerebral vasculature. In wild-type mice, ephrin B2 (brown stain) and eph B4 (brown stain) are observed in endothelial cells and medial SMCs of arteries and veins, respectively (*K* and *N*). Mutant arteries display reduced medial ephrin B2 staining (compare *L* with *K*) with minimal cross-reactivity to veins (*M*). However, mutant arteries do not express eph B4 in medial SMCs (*O*) despite eph B4 staining in bona fide venous structures (compare *O* with *P*). v, vein; a, artery.

Discussion

In the studies described in this report, we expressed DNMAML1 in vSMCs to block canonical Notch signaling in a vSMC-autonomous fashion. Because it acts downstream of Notch receptors, DNMAML1 inhibits the cumulative activity of all Notch receptors expressed on vSMCs, thereby revealing Notch functions that may be obscured when only one Notch receptor or ligand is genetically targeted. SM22-Cre$^+$/DNMAML1$^+$ mutant mice exhibit remarkable abnormalities in cerebrovascular patterning, as well as derangements of arterial architecture. The arterial anatomy of mutant mice is consistent with previous reports implicating Notch signaling in A-V cell-fate decisions. In zebrafish, mutation in the *gridlock* gene (ortholog of *HRT2*) leads to alterations in A-V cell fate (27). Similarly, mice harboring a null mutation in the Notch-3 receptor exhibit reduced SMC mass within arteries and display reduced ephrin B2 expression (28). However, patterning defects of the cerebral vasculature were not observed in Notch-3 null mutants, suggesting that additional Notch receptors expressed in vSMCs also may mediate functions required for cerebrovascular patterning (28). Taken together, these data reveal an unequivocal SMC-autonomous role for Notch signaling in patterning of the cerebral vasculature. These data are consistent with a molecular model, wherein Notch receptors transduce signals from intimal endothelial cells or, more likely, adjacent vSMCs that regulate the proliferative or differentiation capacity and/or survival of vSMCs composing the tunica media of arteries. The conditional transgenic, gene-targeting strategy used in these studies strongly suggests that this signal is transduced through a CSL-dependent Notch signaling pathway.

In vertebrates, the brain is protected from ischemia by primary and secondary collateral vessels (12, 30). The primary collateral vessels form the CW, and they are capable of responding to acute changes in perfusion pressure caused by occlusion of a carotid or vertebral artery (12, 30). By contrast, secondary collateral vessels require time for vessel recruitment, providing an adaptive response to chronic hypoperfusion or cerebral ischemia (12, 14). The profound defects in the CW and other cerebral arteries observed in SM22-Cre$^+$/DNMAML1$^+$ mutant mice strongly suggests that Notch signaling plays a critical role in the patterning of the cerebral vasculature required for primary collateral vessel function. Remarkably, a neurological phenotype consistent with stroke was evoked by unilateral carotid occlusion in the SM22-Cre$^+$/DNMAML1$^+$ mutant mice, but not in control littermates. High-resolution μ-CT brain imaging revealed lack of functional left–right cerebral arterial communication at the CW in the SM22-Cre$^+$/DNMAML1$^+$ mutant mice. This defect in patterning of the CW provides a precise anatomic explanation for the neurological sequelae and death observed in SM22-Cre$^+$/DNMAML1$^+$ mutant mice when cerebral blood flow was restricted by unilateral carotid artery occlusion.

The cerebrovascular circulation has evolved to maintain constant tissue perfusion despite perturbations in blood pressure and volume. Variation in the anatomy of the CW is remarkably common in humans and is associated with excess morbidity and mortality in patients undergoing common surgical procedures involving the carotid arteries, ascending aorta, and the aortic arch (12, 17, 18, 31, 32). The variation in CW anatomy and the patterning of the cerebral vessels in SM22-Cre$^+$/DNMAML1$^+$ mutant mice recapitulate common variations observed in humans (12, 14, 17). These data provide a conceptual framework for examining the role that Notch receptors, Notch ligands, and Notch-regulated target genes play in the genetic variation underlying the heterogeneity of cerebrovascular patterning. It is tempting to speculate that genetic or functional mutations in Notch receptors and/or genes activated by the Notch intracellular domain in vSMCs may be responsible, in part, for a genetic predisposition to stroke. In any case, these data demonstrate that Notch signaling in vSMCs plays a critical role in patterning the CW and cerebral arteries required for the homeostatic response of the cerebral vasculature to regional ischemia.

Methods

Generation of SM22-Cre$^+$/DNMAML1$^+$ Conditional Transgenic Mice. ROSA$^{DNMAML1/DNMAML1}$ mice containing Cre recombinase-dependent expression of DNMAML1–EGFP fusion protein were described previously (19). SM22-Cre transgenic mice expressing Cre recombinase under the transcriptional control of the 2.8-kb mouse SM22α promoter have been described previously (20). Each parental strain was back-crossed seven generations into C57BL/6 genetic backgrounds. Intercrossing ROSA$^{DNMAML1/DNMAML1}$ and SM22-Cre transgenic mice resulted in SM22-Cre$^+$/DNMAML1$^+$ (DNMAML1 expressing) and SM22-Cre$^-$/DNMAML1$^+$ (non-DNMAML1 expressing, control) littermates in normal Mendelian ratios (i.e., 50% progeny contained both a ROSA^{DNMAML1} allele and the cre recombinase transgene) (Fig. 1*A*). All mouse experimentation was performed under approved protocols from the University of Pennsylvania Animal Care and Use Committee and National Institutes of Health guidelines.

Tissue Fluorescence and Immunohistochemistry. Aorta, bladder, and brain were freshly harvested from killed mice immediately after left-ventricular saline injection. Analogous organs from SM22-Cre$^+$/DNMAML1$^+$ and SM22-Cre$^-$/DNMAML1$^+$ mice were paired side by side and subjected to UV irradiation. Green fluorescence from expressed DNMAML1-EGFP was visualized and recorded by using a fluorescence-dissecting microscope. Aorta and brain tissue specimens fixed in 2% paraformaldehyde were either subjected to H&E staining or stained with HRP-conjugated secondary antibody and Hoechst counterstain. Primary antibodies used in the study include anti-GFP (1:100; Molecular Probes, Eugene, OR), anti-Ephrin B2 (1:20; R & D Systems, Minneapolis, MN), and anti-Eph B4 (1:50; R & D Systems). Histology protocols may be assessed on the University of Pennsylvania Molecular Cardiology website at www.med.upenn.edu/mcrc/histology_core/.

Isolation of Primary Aortic SMCs. Aortas from killed adult SM22-Cre$^+$/DNMAML1$^+$ and SM22-Cre$^-$/DNMAML1$^+$ littermate control mice were removed after gentle perfusion with PBS (GIBCO, Carlsbad, CA) and transferred to fresh plates containing 20% FCS (HyClone Laboratories, Logan, UT). Adventitial fat and connective tissue were removed by microdissection, and the aortas were opened along the longitudinal axis. The tissues were then transferred into fresh media (40% Ham's F12, GIBCO; 40% DMEM, GIBCO; 20% FBS, HyClone Laboratories; 1% PCN/Strep, GIBCO; 1% L-glutamine, GIBCO; 2% 20 mM Hepes, GIBCO) with lumen side firmly adherent with an overlying coverslip. Incubation at 37°C (5% CO_2) resulted in vSMC migration from the aortas, and after 2 weeks the cells were passaged. Early passage (2–4) vSMCs were used for the Notch stimulation experiments. Cells stained positively for SM-αActin and the expression of vSMC contractile genes were confirmed by RT-PCR (data not shown).

Notch Ligand Stimulation Assay and Real-Time RT-PCR Analyses. Notch signaling was induced in SM22-Cre$^+$/DNMAML1$^+$ and SM22-Cre$^-$/DNMAML1$^+$ primary aortic SMCs plated on culture dishes displaying immobilized Jagged-1 ligand as described (33). Expression levels of Notch target genes *HRT1*, *HRT2*, and *HRT3* relative to GAPDH were quantified by real-time PCR as described (33). Experiments were conducted on multiple ($n = 4$) aortic SMC isolates.

Carotid Artery Ligation. Mice were anesthetized with Avertin (0.4 mg/g i.p. injection) and placed supine in a clean surgical field. After hair removal, a small midline neck incision and gentle tissue dissection allowed for visualization of the left (or right) common carotid artery proximal to its bifurcation, and the vessel was ligated with 6–0 Prolene (Ethicon, Piscataway, NJ). The wound was closed with suture clips, and the mice recovered from anesthesia.

Carbon Black Perfusion of Cerebrovasculature. Mouse hearts were exposed either under anesthesia or immediately postmortem. After opening the right atrium to ambient pressure, a 21-gauge butterfly needle was inserted into the left ventricle, through which 2 ml of heparinized saline was perfused, followed by 2 ml of 2% paraformaldehyde and 2 ml of carbon black ink. All perfusions were performed in series at 1 ml/min by using an Advance Infusion Pump Series 1200 (CellPoint Scientific, Gaithersburg, MD). Mice were decapitated, the brains were carefully removed, and the CW anatomy was visualized by using a dissecting microscope.

μ-CT Brain Imaging and Sample Preparation. Postmortem perfusion of 2 ml of Microfil (Flowtech, Atlanta, GA) at 1 ml/min was administered after saline perfusion in a manner identical to the carbon black injection protocol described under *Methods*. The intravascular Microfil was allowed to solidify overnight at room temperature, followed by decapitation, scalp removal, and immersion of the intact skull in 10% paraformaldehyde for long-

term fixation. μ-CT brain imaging was performed on an eXplore Locus SP specimen scanner (GE Healthcare, Chalfont St. Giles, U.K.). Scan protocol included 80 keV, 80 μA, 250-μm Al filter, short-scan (Parker, Mayfield Heights, OH) method, 500 views at 0.4° steps, four averages, $8 \times 8 \times 8$-μm^3 reconstruction voxel, and 3.5-h scan time. Image data were analyzed by using MicroView (GE Healthcare), ImageJ (National Institutes of Health, Bethesda, MD), and OsiriX software (www.osirix-viewer.com).

This work was supported by National Institutes of Health Grants K08 HL079072 (to A.P.), K25 EB001427 (to A.C.W.), P01 CA93615 (to W.S.P.), and P01 HL075380 (to M.S.P.).

1. Uyttendaele H, Ho J, Rossant J, Kitajewski J (2001) *Proc Natl Acad Sci USA* 98:5643–5648.
2. Takeshita K, Satoh M, Ii M, Silver M, Limbourg FP, Mukai Y, Rikitake Y, Radtke F, Gridley T, Losordo DW, *et al.* (2007) *Circ Res* 100:70–78.
3. Hellstrom M, Phng LK, Hofmann JJ, Wallgard E, Coultas L, Lindblom P, Alva J, Nilsson AK, Karlsson L, Gaiano N, *et al.* (2007) *Nature* 445:776–780.
4. Carlson TR, Yan Y, Wu X, Lam MT, Tang GL, Beverly LJ, Messina LM, Capobianco AJ, Werb Z, Wang R (2005) *Proc Natl Acad Sci USA* 102:9884–9889.
5. Iso T, Hamamori Y, Kedes L (2003) *Arterioscler Thromb Vasc Biol* 23:543–553.
6. Mumm JS, Kopan R (2000) *Dev Biol* 228:151–165.
7. Fischer A, Gessler M (2003) *Trends Cardiovasc Med* 13:221–226.
8. Bisschops RH, Klijn CJ, Kappelle LJ, van Huffelen AC, van der Grond J (2003) *Neurology* 60:1435–1441.
9. Derdeyn CP, Videen TO, Fritsch SM, Carpenter DA, Grubb RL, Jr, Powers WJ (1999) *Stroke* 30:1019–1024.
10. Hendrikse J, Hartkamp MJ, Hillen B, Mali WP, van der Grond J (2001) *Stroke* 32:2768–2773.
11. Hoksbergen AW, Legemate DA, Csiba L, Csati G, Siro P, Fulesdi B (2003) *Cerebrovasc Dis* 16:191–198.
12. Lee JH, Choi CG, Kim DK, Kim GE, Lee HK, Suh DC (2004) *Am J Neuroradiol* 25:558–564.
13. Rutgers DR, Klijn CJ, Kappelle LJ, van der Grond J (2004) *Stroke* 35:1345–1349.
14. Schomer DF, Marks MP, Steinberg GK, Johnstone IM, Boothroyd DB, Ross MR, Pelc NJ, Enzmann DR (1994) *N Engl J Med* 330:1565–1570.
15. van der Grond J, van Raamt AF, van der Graaf Y, Mali WP, Bisschops RH (2004) *Neurology* 63:1452–1456.
16. Vernieri F, Pasqualetti P, Matteis M, Passarelli F, Troisi E, Rossini PM, Caltagirone C, Silvestrini M (2001) *Stroke* 32:1552–1558.
17. Papantchev V, Hristov S, Todorova D, Naydenov E, Paloff A, Nikolov D, Tschirkov A, Ovtscharoff W (2007) *Eur J Cardiothorac Surg* 31:982–989.
18. Eftekhar B, Dadmehr M, Ansari S, Ghodsi M, Nazparvar B, Ketabchi E (2006) *BMC Neurol* 6:22.
19. Tu L, Fang TC, Artis D, Shestova O, Pross SE, Maillard I, Pear WS (2005) *J Exp Med* 202:1037–1042.
20. Proweller A, Tu L, Lepore JJ, Cheng L, Lu MM, Seykora J, Millar SE, Pear WS, Parmacek MS (2006) *Cancer Res* 66:7438–7444.
21. High FA, Zhang M, Proweller A, Tu L, Parmacek MS, Pear WS, Epstein JA (2007) *J Clin Invest* 117:353–363.
22. Maillard I, Weng AP, Carpenter AC, Rodriguez CG, Sai H, Xu L, Allman D, Aster JC, Pear WS (2004) *Blood* 104:1696–1702.
23. Majid A, He YY, Gidday JM, Kaplan SS, Gonzales ER, Park TS, Fenstermacher JD, Wei L, Choi DW, Hsu CY (2000) *Stroke* 31:2707–2714.
24. Fujii M, Hara H, Meng W, Vonsattel JP, Huang Z, Moskowitz MA (1997) *Stroke* 28:1805–1810.
25. Beckmann N (2000) *Magn Reson Med* 44:252–258.
26. Barone FC, Knudsen DJ, Nelson AH, Feuerstein GZ, Willette RN (1993) *J Cereb Blood Flow Metab* 13:683–692.
27. Zhong TP, Rosenberg M, Mohideen MA, Weinstein B, Fishman MC (2000) *Science* 287:1820–1824.
28. Domenga V, Fardoux P, Lacombe P, Monet M, Maciazek J, Krebs LT, Klonjkowski B, Berrou E, Mericskay M, Li Z, *et al.* (2004) *Genes Dev* 18:2730–2735.
29. Foo SS, Turner CJ, Adams S, Compagni A, Aubyn D, Kogata N, Lindblom P, Shani M, Zicha D, Adams RH (2006) *Cell* 124:161–173.
30. Hartkamp MJ, van Der Grond J, van Everdingen KJ, Hillen B, Mali WP (1999) *Stroke* 30:2671–2678.
31. Bagan P, Vidal R, Martinod E, Destable MD, Tremblay B, Dumas JL, Azorin JF (2006) *Ann Vasc Surg* 20:747–752.
32. Hendrikse J, Rutgers DR, Klijn CJ, Eikelboom BC, van der Grond J (2003) *Stroke* 34:1650–1654.
33. Proweller A, Pear WS, Parmacek MS (2005) *J Biol Chem* 280:8994–9004.